




Tunable Microwave Absorbing Properties of $\text{CoFe}_2\text{O}_4/\text{PANI}$ Nanocomposites

K. PRAVEENA ^{1,3} and M. BOUODINA²

1.—Department of Physics, Palamuru University, Mahabubnagar, Telangana State 509001, India.
2.—Department of Physics, College of Science, University of Bahrain, PO Box 32038, Sakheer, Kingdom of Bahrain. 3.—e-mail: praveenaou@gmail.com

The design of $\text{CoFe}_2\text{O}_4/\text{PANI}$ interfaces can significantly enhance a material's dielectric loss ability at high frequency. This paper presents a simple method to generate $\text{CoFe}_2\text{O}_4/\text{PANI}$ interfaces to enhance microwave absorption and attenuation at high frequency. Cobalt ferrite nanoparticles were mixed with PANI at various wt.%. X-ray diffraction of nanocomposites indicates that the structure of the core material has a spinel structure and demonstrates the formation of $\text{CoFe}_2\text{O}_4/\text{PANI}$ nanocomposites. The particle size of ferrite and polyaniline powders were measured using transmission electron microscopy. The particle size of CoFe_2O_4 is found to be 20 nm. The saturation magnetization (M_s) of all the nanocomposites were found to be decreasing with decrease of ferrite content, while coercivity (H_c) remained at the value corresponding to pure cobalt ferrite. Because the $\text{CoFe}_2\text{O}_4/\text{PANI}$ interface induces a strong dielectric loss effect, all of these materials achieved broad effective frequency width at a coating layer as thin as 1.9 mm. The complex permittivity (ϵ' and ϵ'') and permeability (μ' and μ'') were collected by a vector network analyser and the absorbing properties were calculated according to transmission theory. ϵ' , ϵ'' and μ'' increases with an increase of PANI, whereas μ' decreases. The absorption peak shifted to the high-frequency side with PANI. These results showed that a wider absorption frequency range could be obtained by adding different polyaniline content in cobalt ferrite.

Key words: Ferrites, polyaniline, complex permittivity, complex permeability, reflection coefficient, microwave absorption

INTRODUCTION

With the rapid development in miniaturization and densification of electronic products,^{1,2} the severe heat dissipation problem has become a serious issue affecting stability and reliability,^{3,4} thereby making electromagnetic interference (EMI) a more serious issue that affects human health and interferes with the normal operation of other electronic devices.⁵ To address this problem, magnetic + polymer nanocomposites known as high-

performance electromagnetic wave absorbing materials are of great interest to scientists due to their ease of preparation, low cost, large magnetic momentum, reliability and high electrical resistivity.⁶

Hence, there is a desire for the development of high-performance electromagnetic wave absorbing materials. These materials have drawn worldwide attention because they are able to attenuate EM wave energy by converting it into thermal energy.^{7,8} Ideally, electromagnetic wave absorption materials should have strong absorption capability, broad absorption bandwidth, thin matching thickness, and be light weight.⁹

(Received January 20, 2020; accepted July 22, 2020; published online August 11, 2020)

High-performance magnetic absorbers are designed through three strategies.

1. The first strategy is to make core/shell structures, where magnetic materials are used as the core and the dielectric materials as shell. However, this requires careful synthesis routes and the scale-up synthesis is always a problem.⁹
2. The second strategy is to simply mix magnetic materials with high dielectric property materials. This strategy is quite easy to perform, since the synthesis of the two materials is achieved separately and the synthesis can be scaled up readily. If the mixing of two materials is not homogeneous, the impedance matching might not be achieved as desired.⁹
3. The third strategy is to assemble magnetic nanomaterials onto 2D nanomaterials such as graphene to form a hybrid structure. Graphene is a high dielectric material, but it cannot be used alone due to the limitation in impedance matching with the absorber matrix. Thus, it is often combined with magnetic materials.⁹

Magnetic materials with permeability and high saturation magnetization such as Co, Mn, and Zn, and ferrites were used as microwave absorbing materials.^{10–12} The magnetic ferrites are mostly used due to their low eddy current losses and high electrical resistivity.

Polyaniline (PANI) is one of the most popular conducting polymers among the large family of intrinsically conductive polymers due to its easy synthesis, cheap raw material, good environmental and thermal stability, high electrical conductivity¹³ and negative permittivity.¹⁴ PANI has promising applications in biosensors,¹⁵ soft tissue engineering,¹⁶ electrochromics,¹⁷ electromagnetic interference (EMI) shielding¹⁸ and has attracted great interest as a new functional component to produce multifunctional composites (Table I).^{19–21}

In brief, the preparation methods of these nanocomposites can be classified in four main routes proposed in the literature that are graphically represented in Fig. 1 for the preparation of composites based on PANI.³²

- (1) In this route, polymer and magnetic nanoparticles were synthesized separately and then mixed to produce nanocomposites. This route is not suitable for conducting polymers and this method leads to heterogeneous composites with large agglomeration of particles; therefore, it is not commonly used.³²
- (2) The second route is in situ preparation of both the polymer and the magnetic nanoparticles and is not yet very commonly used, although it is simple and rapid, because of its poor control over the polymer and the magnetic nanoparticles.³²

- (3) The third route is the most commonly used. First nanoparticles are synthesized and then the polymerization is carried out in situ in the presence of the nanoparticles. Therefore, it is possible to synthesize nanoparticles in a controlled manner and at the same time produce homogeneous nanocomposites.³²
- (4) The fourth route is synthesis of nanoparticles within the PANI previously synthesized, which provides nanocomposites more homogeneous. But, controlling the size of the nanoparticle and the solubility of the polymer is also an issue.³²

Polymer nanocomposites are prepared by blending or mixing the different components in solution or in a melting process. Very few are reported related to the fabrication of nanocomposites based on conducting polymers using a solution method. In these cases, the polymer must be soluble or emulsifiable in the solvent and also the magnetic nanoparticles must be colloidal stable in order to avoid the agglomeration in the final product (Fig. 2).³²

Ma et al have synthesized $\text{Co}_{0.5}\text{Zn}_{0.5}\text{Fe}_2\text{O}_4/\text{PANI}$ by in situ polymerization in an aqueous solution and studied their microwave absorption studies. The synthesized nanocomposites showed that maximum reflection loss (RL) of the $\text{PANI}/\text{Co}_{0.5}\text{Zn}_{0.5}\text{Fe}_2\text{O}_4$ nanocomposite was about -39.9 dB at 22.4 GHz with a bandwidth of 5 GHz.³³

Sulaiman et al reported $\text{Co}_{0.5}\text{Zn}_{0.5}\text{Fe}_2\text{O}_4/\text{PANI}$ -PTSA nanocomposites and studied the microwave absorption properties in the X-band. They reported a maximum RL of -2.3 dB ($> 40\%$ power absorption) at 8.1 GHz, -17.08 dB (98% power absorption) at 9 GHz and -24.86 dB (99.73% power absorption) at 10.9 GHz.³⁴

Choudhary et al have synthesized $\text{Ba}_x\text{Pb}_{1-x}\text{Fe}_{12}\text{O}_{19}/\text{PANI}$ nanocomposites and reported the microwave absorption studies in the X- and Ku-bands. They demonstrated that incorporation of hexaferrite powder in a PANI-based composite results in a superior SE_T value of ~ 19 – 24 dB (18 GHz).³⁵

Apart from magnetic materials with PANI nanocomposites, researchers are working towards the development of EMI shielding materials including Zhang et al.³⁶, who fabricated ultra-thin and flexible $\text{Ti}_3\text{C}_2\text{T}_x/\text{co-doped polyaniline}$ and reported the EMI shielding effectiveness (SE) of the composite film as 36 dB. Yang et al.³⁷ fabricated a 3D copper nanowires-thermally annealed graphene aerogel (CuNWs-TAGA) framework, and this epoxy nanocomposite exhibited a maximum EMI SE value of 47 dB. Song et al.³⁸ prepared honeycomb structural rGO-MXene/epoxy nanocomposites and they obtained an EMI SE of 55 dB. Tong et al.³⁹ have fabricated an artificial suede-like cloth (ASC)/PANI fabric which exhibits an effective EMI shielding capability of 25.90 dB.

Table I. Some of the most relevant examples of magnetic nanoparticles based with PANI nanocomposites, with respective their properties and applications

Polymer	Magnetic material	Properties studied	References
PANI	Ni-doped cobalt ferrite Cd ²⁺ substituted nickel ferrite	High-performing shielding candidate for EMI applications Maximum SE _T (42.7 dB) in the X-band range	Ref. 22 Ref. 23
	BaFe ₁₂ O ₁₉ and reduced graphene oxide (rGO)	Effective microwave-absorption bandwidth for reflection loss below - 10 dB was 0.9 GHz from 8.2 GHz to 9.1 GHz with the thickness of 2.6 mm	Ref. 24
	CoRE _x Fe _{2-x} O ₄ (RE = La, Ce, Y, x = 0.05–0.25)	Preparation and microwave-absorbing properties	Ref. 25
	Ni _{0.6} Zn _{0.4} Fe ₂ O ₄	Controlled synthesis and microwave-absorption properties	Ref. 26
	Mn _{0.2} Ni _{0.4} Zn _{0.4} Fe ₂ O ₄	Enhanced microwave-absorption properties in the X-band	Ref. 27
	Polyaniline/(1 - x) Ba- Fe ₁₂ O ₁₉ /CaFe ₂ O ₄ /xCo- Fe ₂ O ₄	Microwave-absorbing properties	Ref. 28
	MnFe ₂ O ₄	Microwave-absorbing properties	Ref. 29
	NiZn ferrite	Microwave-absorbing properties in 2–40 GHz	Ref. 30
	Ni _{0.5} Zn _{0.5} Fe ₂ O ₄	Microwave-absorbing properties in 2–18 GHz	Ref. 31

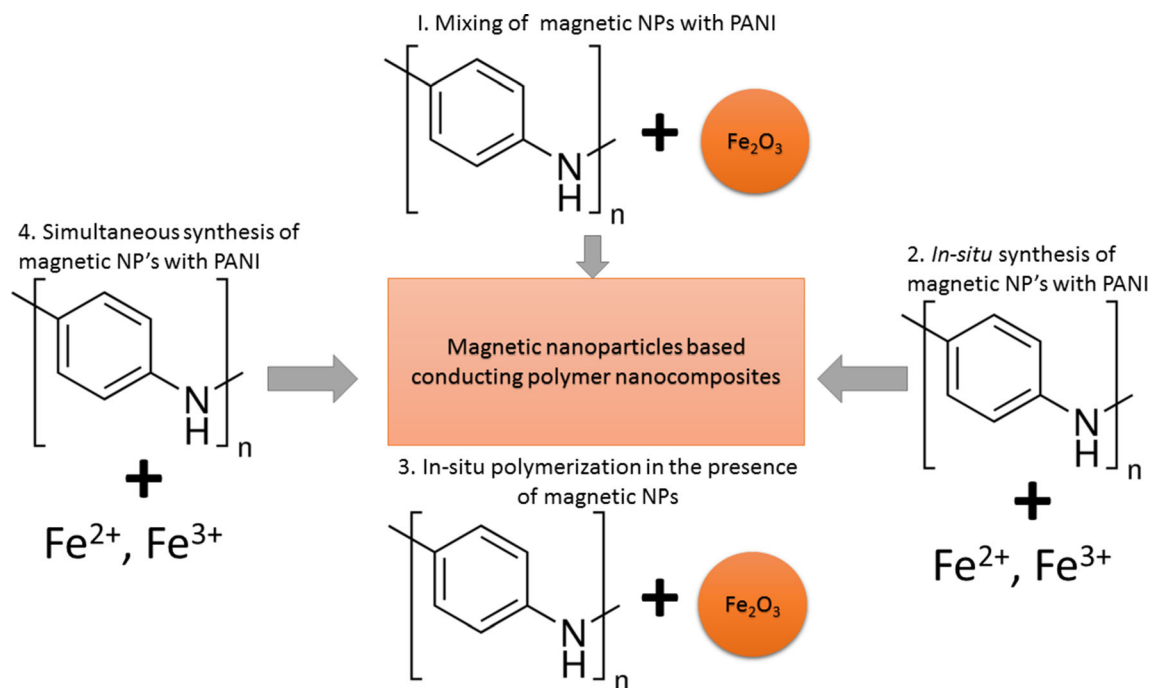


Fig. 1. Scheme of the different preparation methods of magnetic nanoparticles-based conducting nanocomposites.

In this article, we report an approach to generate ferrite/polymer interfaces by preparing nanocomposites of cobalt ferrite (CF) with polyaniline (PANI). The ferrites were synthesized through an aqueous co-precipitation method. This report is an adaptation of the Yang method⁴⁰ which is helpful in synthesizing high specific surface area cobalt ferrite nanoparticles. The reported method is a green and viable alternative to other synthesis techniques currently used which (among others) include a microwave hydrothermal method,^{41–43} sol-gel,⁴⁴

forced hydrolysis,⁴⁵ combustion,⁴⁶ micro-emulsion⁴⁷ and a mechano-chemical method.⁴⁸

EXPERIMENTAL

Synthesis of Cobalt Ferrite

The nanoparticles of CoFe₂O₄ (CF) was prepared using high purity (99.9%) cobalt nitrate [Co(N-O₃)₂·6H₂O] and ferric nitrate [Fe(NO₃)₃·9H₂O] solutions taken in stoichiometric ratio. These reagents were dissolved in 50 mL of de-ionized water. An aqueous NaOH (99.99%) solution was added to the

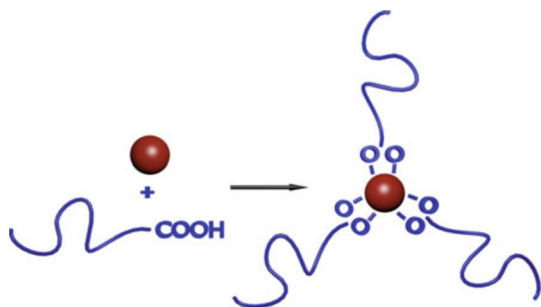


Fig. 2. Illustrative representation of the conducting nanocomposites prepared from pre-synthesized conducting polymers and magnetic NPs.

mixture to maintain pH \sim 9.4. The mixture was stirred at 60°C for 2 h. The precipitate was washed repeatedly with de-ionized water, followed by drying in an oven overnight at 60°C.⁴⁹

Synthesis of CoFe₂O₄/PANI Nanocomposites

The preparation of CoFe₂O₄/PANI nanocomposites is as follows: 11.88 mL aniline (99.5% purity) was dissolved in 150 mL of distilled water containing 25 mL hydrochloric acid. The desired quantity of CoFe₂O₄ was added to the solution and stirred thoroughly, and the solution was precooled at 0°C. Ammonium peroxydisulfate of (APS) 98% purity (27.38 g, dissolved in 1.8 M HCl solution) was slowly added to the reaction mixture. During the synthesis, the mixtures were stirred at 400–500 rpm for 16 h and the temperature was maintained at 0°C. The precipitated powder was centrifuged and washed with distilled water until the filtrate became colourless and then dried in a vacuum drying cabinet at 100°C for 24 h. The samples were designated CF/PANI-10, CF/PANI-20, CF/PANI-30, CF/PANI-40 and CF/PANI-50 for 10 wt.%, 20 wt.%, 30 wt.%, 40 wt.% and 50 wt.% of ferrite loading, respectively.⁴⁹

Characterizations

The phase identification of the samples was performed with XRD with Cu K_α ($\lambda = 1.54 \text{ \AA}$) radiation. The lattice constant (a) for the cubic crystal system was calculated using the equation $a = d\sqrt{h^2 + k^2 + l^2}$ where $h k l$ are the Miller indices of the diffraction peak and d is the interplanar spacing. The theoretical densities ($d_{x\text{-ray}}$) were calculated from the values of lattice parameters by the relation $d_{x\text{-ray}} = \frac{8M}{Na^3} \text{ g/cm}^3$ where 8 is the number of formula units in a unit cell, M is the molecular weight, N is the Avogadro number and ' a ' is a lattice constant. The bulk density of the present samples was measured using the Archimedes principle. The particle size of as prepared powders was studied by using transmission electron microscopy (TEM, JEOL, Japan). Field emission scanning electron microscope (FE-SEM) analysis was carried out to

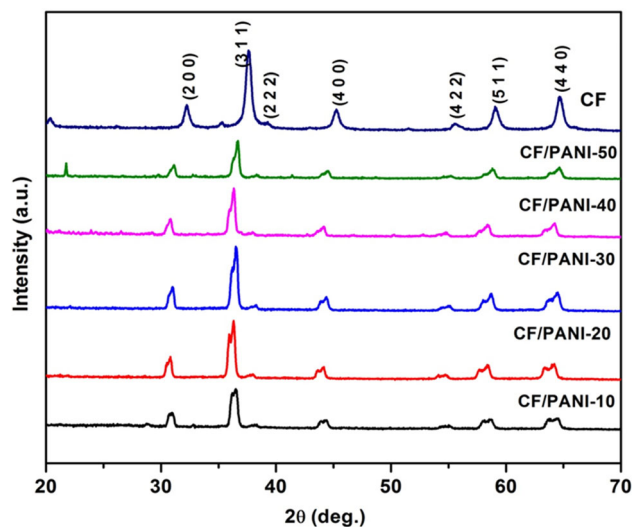


Fig. 3. XRD patterns of CoFe₂O₄-PANI with different ferrite loadings.

study the morphological characteristics using an INSPECT™ S50. The magnetic nature was confirmed by magnetization measurements using a vibrating sample magnetometer (Lake Shore, USA) up to 6 kOe.⁴⁹ The frequency dependence of complex permittivity and permeability and reflection coefficient for the specimen were carried out using an Agilent 8517B Vector Network Analyser (VNA) in the 2–20 GHz range. The complex permittivity and permeability of the specimens were obtained using the scattering parameters using the algorithm of Weir⁵⁰, Nicolson and Ross⁵¹. In the present work, electron paramagnetic resonance (EPR) spectroscopy is employed in the microwave region of the electromagnetic spectrum X-band (9.8 GHz) using a JEOL Spectrometer. The detailed information regarding VNA and EPR spectroscopy available as Supplementary information.^{52–54}

RESULTS AND DISCUSSION

Figure 3 shows the XRD patterns of the CoFe₂O₄ and different loadings of PANI matrix. The diffraction peak positions were consistent with the CoFe₂O₄. From the figure we can see the characteristic peak of CoFe₂O₄ at (3 1 1) plane. The lattice constants of nanocomposite samples are given in Table II. The increase of lattice constant with ferrite concentration is attributed to the close interaction between polymer chains and incorporated ferrite nanocrystals. The (3 1 1) plane is shifting towards the higher angle side with an increase of ferrite content, which is due to the stress incorporated by ferrite particles. In general, polycrystalline ferrite consists of separate grains in the form of polyhedrons with clear-cut boundaries, and the average grain size varies between 30 to 45 nm; after coating with PANI a continuous over-layer of conducting polymer is produced on the ferrite

Table II. Data of lattice constant, bulk density, X-ray density and porosity of CF/PANI with different PANI loadings

Composition	Sample name	Lattice constant <i>a</i> (Å)	Bulk density (g/cm ³)	Bulk density (g/cm ³)	Porosity (%)
CoFe ₂ O ₄	CF	8.342	5.28	5.12	3
50 wt.% CoFe ₂ O ₄ + 50 wt.% PANI	CF/PANI-50	8.336	5.10	5.30	4
40 wt.% CoFe ₂ O ₄ + 60 wt.% PANI	CF/PANI-40	8.326	5.00	5.42	8
30 wt.% CoFe ₂ O ₄ + 70 wt.% PANI	CF/PANI-30	8.320	4.91	5.50	11
20 wt.% CoFe ₂ O ₄ + 80 wt.% PANI	CF/PANI-20	8.318	4.80	5.62	15
10 wt.% CoFe ₂ O ₄ + 90 wt.% PANI	CF/PANI-10	8.310	4.72	5.70	18

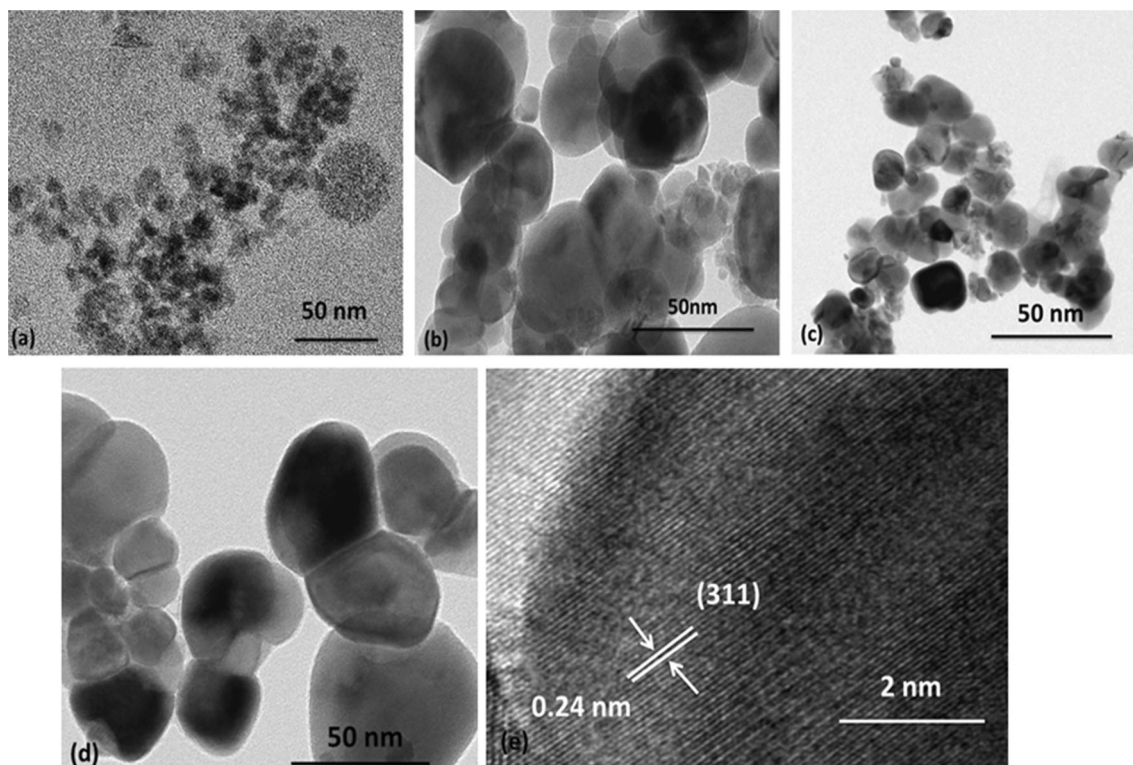


Fig. 4. (a) Low-magnification HRTEM image of CF/PANI-10, (b) CF/PANI-20 nanocomposites, (c) CF/PANI-30 nanocomposites, (d) CF/PANI-40 nanocomposites, (e) high-magnification HRTEM image of CF/PANI-10 showing the (3 1 1) oriented lattice planes of cobalt ferrite.

particle surface which is deposited at the crystallite boundaries and covers the surface defects such as pores and cracks (this can be observed from TEM images).^{49,55}

Figure 4a, b, c, d and e shows the TEM and high-resolution (HR) TEM images of CoFe₂O₄ and CF/PANI nanocomposites, respectively. Figure 4a demonstrates the low magnification of HRTEM of CF/PANI-10. It is very clear that PANI and

CoFe₂O₄ are well dispersed. The TEM images of CF/PANI-20 nanocomposites (Fig. 4b), the TEM images of CF/PANI-30 nanocomposites (Fig. 4c), CF/PANI-40 (Fig. 4d), nanocomposites and HRTEM images of CF/PANI-10 (Fig. 4e) exhibits the incorporation of ferrite nanoparticles in the polyaniline matrix. The lattice spacing of 0.24 nm corresponding to the (3 1 1) plane confirms the presence of crystalline CoFe₂O₄ nanoparticles in the amorphous

polymer matrix (Fig. 4c). Table III gives the particle size of CF/PANI with different PANI loadings.⁴⁹

The addition of oxidant APS to the micellar solution of aniline with CoFe_2O_4 leads to the oxidative polymerization of aniline which oxidizes to form anilinium radical cations. The anilinium radical cations subsequently combine with another unit to form neutral dimers. The further oxidation

of these dimers leads to the formation of trimers and finally to a polymer nanocomposite.⁵⁶

Figure 5a, b, c, d, e and f shows the FE-SEM micrographs for the CoFe_2O_4 /PANI nanocomposites and CoFe_2O_4 , respectively. It can be observed from this figure that PANI presents a sponge shape with an average grain size of 50 nm. In Fig. 5b, it is found that the CoFe_2O_4 /PANI nanocomposite (40 wt.%) retains the spongy like morphology, i.e. PANI. It is unknown how to form a sponge-shaped composite in the polymerization process (Fig. 5c). It can

Table III. Particle size (from TEM) of CF/PANI with different PANI loadings

Sample name	Particle size (nm)
CF	20
CF/PANI-50	24
CF/PANI-40	27
CF/PANI-30	21
CF/PANI-20	29
CF/PANI-10	30

Table IV. Atomic weight of CoFe_2O_4

Element	Weight%	Atomic%
O K	23.30	52.16
Fe K	36.12	23.17
Co K	40.58	24.67
Total	100.00	

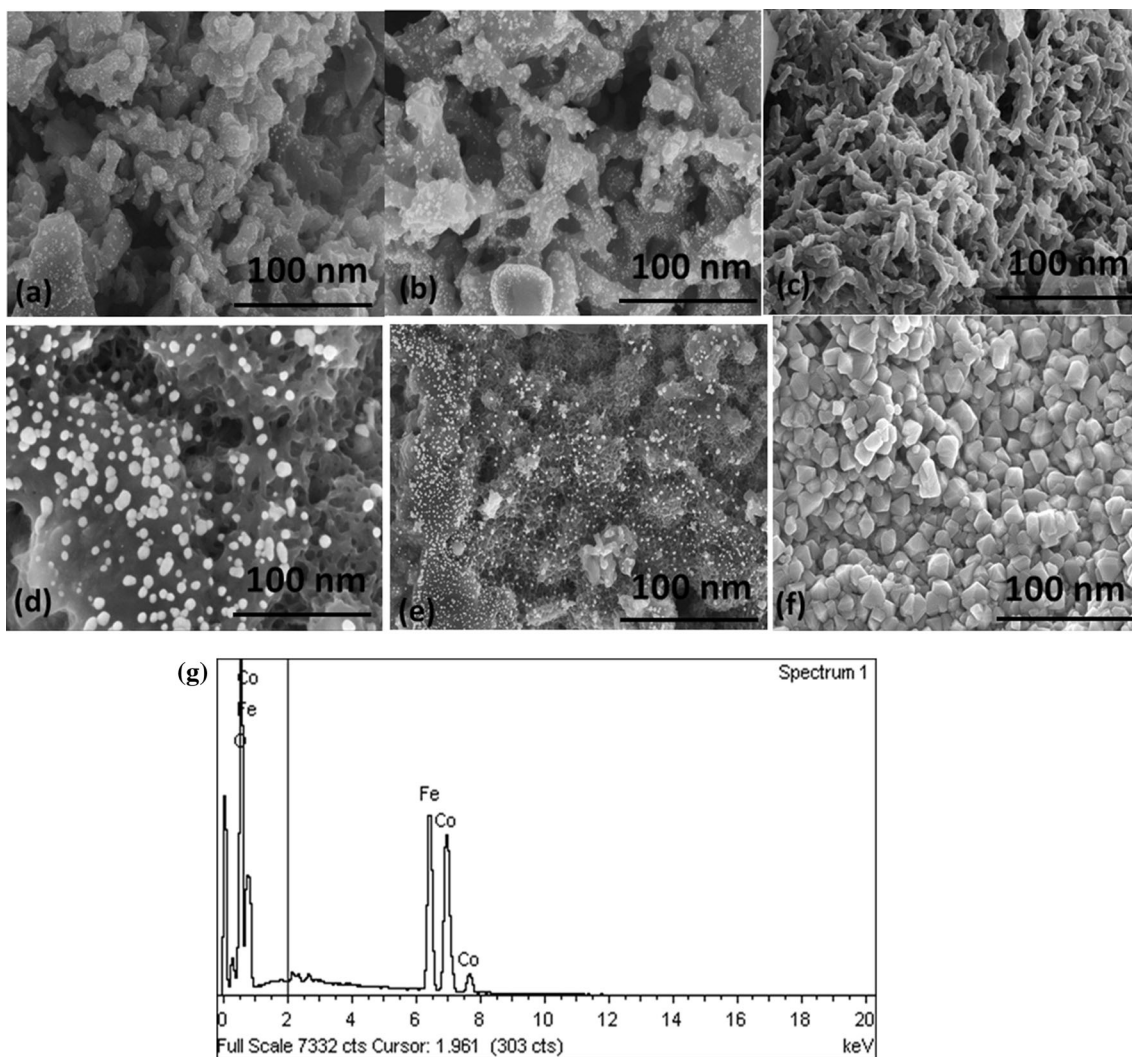


Fig. 5. FE-SEM micrographs of (a) CF/PANI-50, (b) CF/PANI-40, (c) CF/PANI-30, (d) CF/PANI-20, (e) CF/PANI-10, (f) CF, (g) EDAX of CoFe_2O_4 .

be seen from the image of CF/PANI-20 nanocomposites that the CoFe₂O₄ nanoparticles are dispersed on the surface of PANI nanoparticles (Fig. 5d). As shown in Fig. 5f, CoFe₂O₄ nanocrystals possess spherical shape. The average particle size observed is close to the values obtained using the Scherrer formula. Hence, it is very likely that each of the observed particles is a single crystallite. The grain size of CoFe₂O₄ is about 50–60 nm, and the average diameter is in the range of 50–60 nm. The FE-SEM micrographs clearly shows that the CoFe₂O₄ was distributed rather homogeneously and ultrasonication is effective for dispersing ferrite in the polymer matrix. Compositional determination was performed by energy dispersive X-ray (EDAX) analysis, showing peaks corresponding to Co, Fe, and O atoms of the CF sample (Fig. 5g). Table IV shows the atomic weight of CoFe₂O₄ and Fig. 5g EDAX of CoFe₂O₄.

Figure 6 shows the hysteresis loops of CoFe₂O₄ and CF/PANI-10, -20, -30, -40 and -50 samples at room temperature. The values of M_s and H_c are listed in Table V. It can be seen from the figure that M_s values of CF/PANI nanocomposites were less than that of CoFe₂O₄ and decreased with an increase of PANI content. The ferrite is shown to be in a ferrimagnetic phase, while PANI is a nonmagnetic medium. According to the equation $M_S = \phi m_s$,⁵⁷ M_S is related to the wt.% of the magnetic particles (ϕ) and the saturation moment (m_s) of a single particle. It is considered that the saturation magnetization of CF/PANI nanocomposites depends mainly on the wt.% of the magnetic ferrite particles. In addition, nonmagnetic PANI plays a part in isolating the magnetic particles, which results in the transformation of the colinear ferrimagnetic order of ferrite into a noncolinear arrangement and disruption of ferrimagnetic order.⁵⁷ As PANI content increases, the diamagnetic effect is notable. Therefore, the saturation magnetization of CF/PANI nanocomposites is less than that of pure ferrite particles and decreases with the decrease of CoFe₂O₄ content.⁴⁹

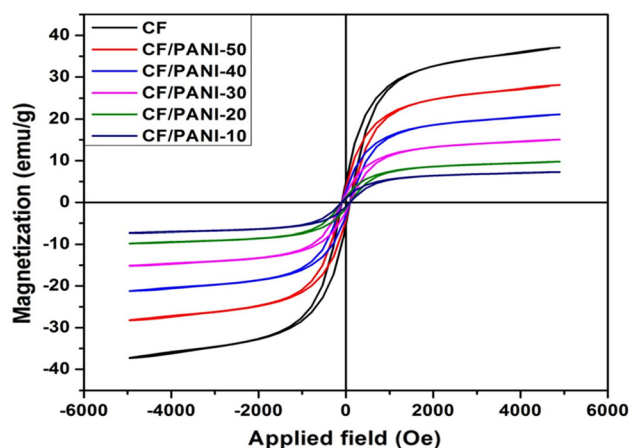


Fig. 6. M-H loops of CF/PANI nanocomposites.

It can be seen from the Table that the values of coercivity of CoFe₂O₄ and CF/PANI nanocomposites are very low. The coercivity of magnetic materials is related to its micro-organizational structures (particle size, particle shape, etc.), magnetic anisotropy (magnetocrystalline, stress, shape), and coated state between phases besides the attribute of the substance itself. Furthermore, PANI is deposited on the ferrite surface and crystallite boundary in the polymerization process, which has a healing effect

Table V. Data of saturation magnetization and coercivity of CF/PANI with different PANI loadings

Sample name	M_s (emu/g)	H_c (Oe)
CF	38	68
CF/PANI-50	26	67
CF/PANI-40	22	67
CF/PANI-30	16	67
CF/PANI-20	8	67
CF/PANI-10	6	65

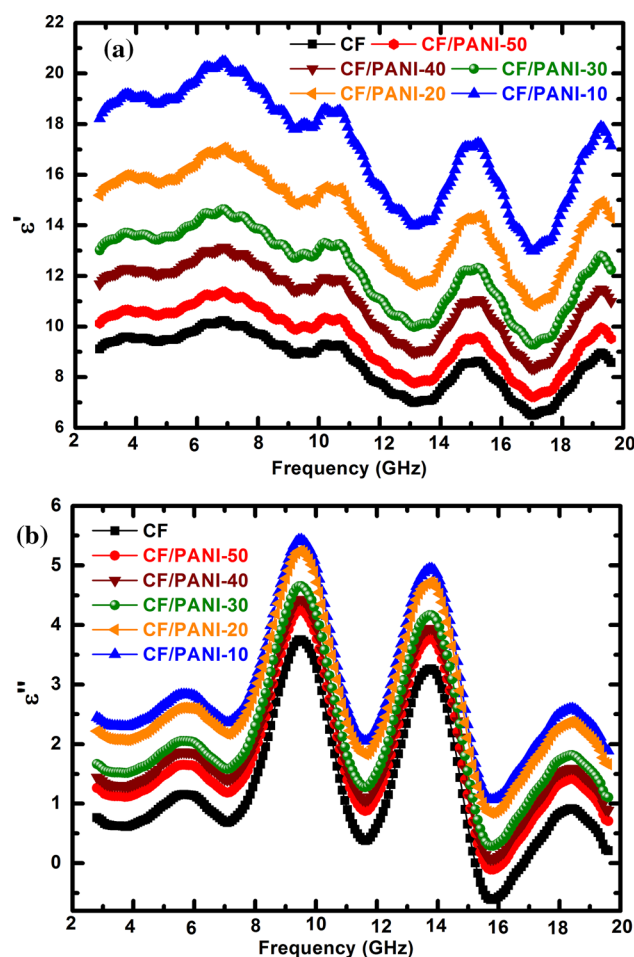


Fig. 7. Frequency dependence of (a) real (ϵ') and (b) imaginary (ϵ'') parts of permittivity.

on the ferrite surface defects, such as pores and cracks, and leads to a decrease in magnetic surface anisotropy of ferrite particles. Consequently, CF/PANI nanocomposites present a lower value of coercivity.⁴⁹

The real part of permittivity (Fig. 7a) (ϵ') depends mainly on the polarization in the polymer backbone and the interfacial polarizations among the ferrite nanoparticles and polyaniline.⁵⁸ When PANI is added to CoFe_2O_4 , more intrinsic polarization and interfacial polarization were generated, so the real part of permittivity increases. The metal ions and defects on the ferrite and the interface between ferrite and PANI result in interfacial polarization. In addition, more PANI generates more interfacial and intrinsic electric dipole polarization, increasing the dielectric constant and the dielectric loss.⁵⁹ Although changes in dielectric constant have been attributed to increased electrical conductivity, a direct correlation was not completely observed in the current study; therefore, the permittivity changes observed in the current study must depend on PANI dispersion. It is known that interfacial polarization density at the polymer filler interface increases with increasing specific surface area of conductive fillers^{60,61} and interfacial polarization can influence the relaxation of polymeric chains and chain segments around the fillers; therefore, samples with better PANI dispersion have a greater dielectric constant.^{60,61}

The imaginary part of permittivity (Fig. 7b) (ϵ'') is attributed to the free ionic, electronic, dipole polarization, space charge polarization and interfacial polarization.^{62,63} As Truong and co-workers reported,⁶⁴ the imaginary part (ϵ'') of permittivity of the composite can be defined by equation:

$$\epsilon'' = \sigma_{dc}/\omega\epsilon_0 + \epsilon''_{ac}$$

where σ_{dc} is the dc conductivity, ω is the angular frequency, which is directly proportional to measured frequency, ϵ_0 is the permittivity of free space, and ϵ''_{ac} is the loss due to high frequency above 8 GHz.^{65,66}

The higher ϵ' and ϵ'' values are observed over the whole frequency range. These higher values imply relatively strong storage capability and dissipative ability of EM energy, which can be readily attributed to the high electrical conductivity and multiple polarization originating from the nanocomposites.⁶⁷ However, it should be noted that the excessively high values in the low-frequency range may give rise to poor impedance matching.⁶⁷ In addition, the ϵ' and ϵ'' values show a similar variation tendency: the ϵ' values increase from 9.16 to 18.58, while the ϵ'' values increase from 3.29 to 5.06 from CoFe_2O_4 to CF/PANI-50 at 10 GHz.

Figure 8a and b shows the real part (μ') and imaginary parts (μ'') of complex permeability. As the frequency is increased from 2 to 20 GHz, μ' values of the nanocomposites experience a rapid

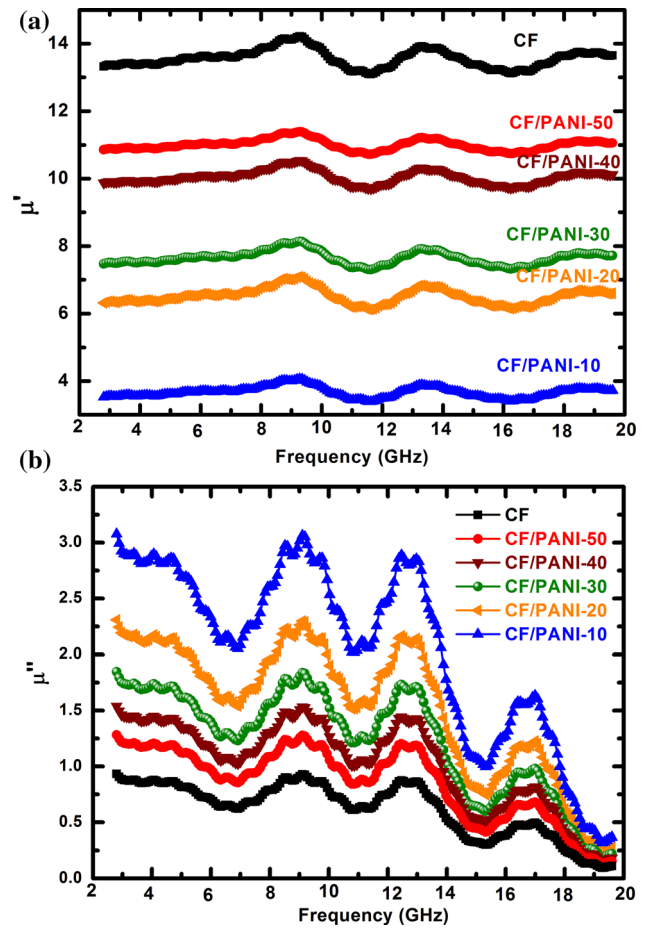


Fig. 8. Frequency dependence of (a) real (μ') and (b) imaginary (μ'') parts of permeability.

Table VI. The values of complex permittivity and permeability values at 10.2 GHz

Sample name	ϵ'	ϵ''	μ'	μ''
CF	9.16	3.29	13.0	0.81
CF/PANI-50	10.06	3.50	11.12	1.03
CF/PANI-40	11.8	3.70	10.07	1.37
CF/PANI-30	13.08	3.96	7.83	1.61
CF/PANI-20	15.26	4.55	6.74	1.99
CF/PANI-10	18.58	5.06	3.71	2.52

decrease from 13.0 to 3.71 from CoFe_2O_4 to CF/PANI-50, and there are minor fluctuations over 2–20 GHz. Because of the higher initial values (> 1.6) of the real part, large μ' values are maintained over the whole frequency range, which is beneficial to maintain a promising impedance matching.⁶⁸ Both μ' and μ'' values increase first and then decrease in three frequency regions (1) 7.8–10.2 GHz, (2) 11.8–14 GHz and (3) 15.8–18 GHz. The μ' value at 10 GHz for CF is 13, and as PANI is added it decreases to 11.12 for CF/PANI-50. Similarly, μ'' varies from 0.81 to 1.03. Table VI demonstrates the

complex permittivity and permeability values at 10.2 GHz.

There are three main mechanisms that contribute to the shielding effectiveness. On one hand, the incident wave is reflected from the surface of the shield, and on the other hand, the shield material absorbs part of the radiation and the third mechanism is based in multiple reflections which can either support or hide the effectiveness, as shown in Fig. 9.³²

Figure 10 shows the frequency dependence of reflection loss of the CoFe₂O₄ and PANI nanocom-

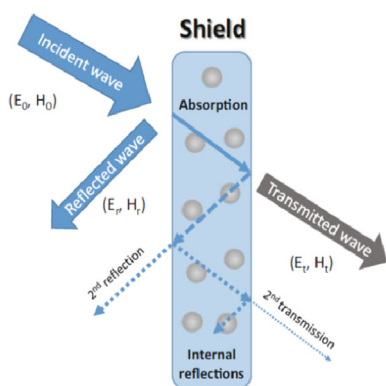


Fig. 9. Schematic representation of the EMI shielding.

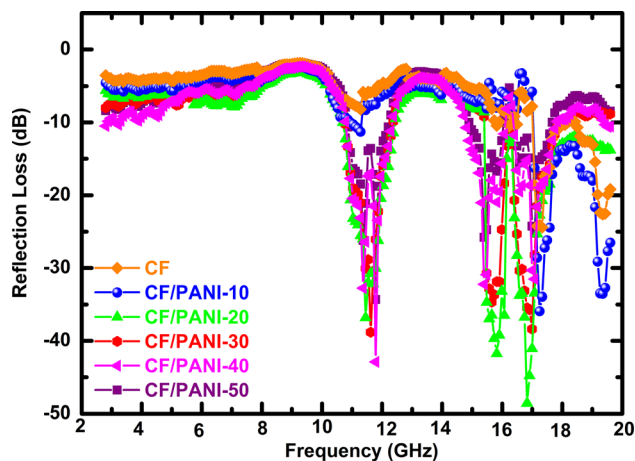


Fig. 10. Microwave absorbing properties of cobalt ferrite and PANI nanocomposites in 2–20 GHz.

posite in the frequency range of 2–20 GHz. It can be seen that CF/PANI nanocomposites have a more obvious effect on microwave absorbing properties than cobalt ferrite nanocomposite at 2–20 GHz. The specimen of the cobalt ferrite showed only one band at 17.1 GHz with -24.2 dB in reflection loss. Among the CF/PANI nanocomposites, the powder prepared from the PANI content of 70, 80 wt.% (CF/PANI-30, CF/PANI-20 nanocomposites) exhibited pronounced absorption bands at 10.4 GHz, 15.8 GHz, 16.4 GHz with the reflection losses of -38.8 dB, -34.6 dB, -38.4 dB, whereas for CF/PANI-20 the absorption appears at 11.8 GHz, 15.8 GHz, 16.9 GHz with reflection losses of -36.9 dB, -41.9 dB, -48.4 dB. Clearly demonstrated (Table VII) is that the intensity and frequency of the reflection loss maximal for the nanocomposite also depend on the PANI content. Meanwhile, the centers of the reflection loss peaks for CF/PANI nanocomposites move gradually to the higher frequencies, which may also be attributed to the enhanced PANI content.

Recently reported literature of EMI SE is as follows:

Jia et al.⁶⁹ reported an EMI SE of 20.7 dB for CA/AgNW/PU film.

Wang et al.⁷⁰ reported EMI SE of 41 dB for Ti₃C₂T_x/epoxy nanocomposites.

Liu et al.⁷¹ fabricated the leaf-like nanostructure is composed of silver nanowires (AgNWs) and transition metal carbide/carbonitride (MXene), and they obtained an outstanding EMI shielding efficiency of 54 dB in the X-band.

Song et al.⁷² have fabricated reduced graphene oxide (rGH) with honeycomb structure and successfully achieved an EMI SE of 38 dB in the X-band.

Shen et al.⁷³ have fabricated carbon scaffolds based on natural wood via a sequential delignification and carbonization process and then used them to prepare EP/carbon composite to exhibit high EMI SE of 27.8 dB in the X-band region.

Liang et al.⁷⁴ have fabricated three-dimensional Fe₃O₄ decorated carbon nanotubes/reduced graphene oxide foam/epoxy (3D Fe₃O₄-CNTs/rGF/EP) nanocomposites and obtained an EMI SE value of 36 dB within the X-band range.

Table VII. The values of absorption bands observed at three different frequency regions

Sample name	RL (– dB) at 11.8 GHz	RL (– dB) at 15.8 GHz	RL (– dB) at 16.9 GHz
CF	8.5	–	–
CF/PANI-50	34.4	25.7	24.7
CF/PANI-40	43.1	32.3	31.5
CF/PANI-30	38.9	34.7	38.4
CF/PANI-20	36.9	41.9	48.6
CF/PANI-10	11.7	–	36.1

Wang et al.⁷⁵ have made few-layered $\text{Ti}_3\text{C}_2\text{T}_x$ MXene fabricated by ionic intercalation and a sonication-assisted method and succeeded in obtaining an EMI SE of 41 dB.

Compared to the above literature, CoFe_2O_4 and PANI nanocomposites are the best materials for microwave absorption because the synthesis of these nanocomposites is very easy and rapid compared to the above methods and materials.

The EPR spectra of CF/PANI nanocomposites were recorded at room temperature, and the dependence on PANI content is shown in Fig. 11. The parameters (ΔH_{PP} , g factor and T_2) obtained from Fig. 11 are given in Table VIII. The EPR spectra show a broad signal; the overlap for the broad signal associated with the free or interactive cobalt ferrite clusters with PANI was gradually discerned. The g value of the CF/PANI nanocomposites and PANI lies in between 2.76 and 2.10, which is closer to that of the free electron.^{30,76,77} Moreover, the value of ΔH_{PP} of PANI is smaller than that of the CF/PANI nanocomposites, and ΔH_{PP} decreases with increasing PANI content (Table VIII). The results may be due to the interaction between cobalt ferrite crystallites and PANI reducing the magnetic dipolar

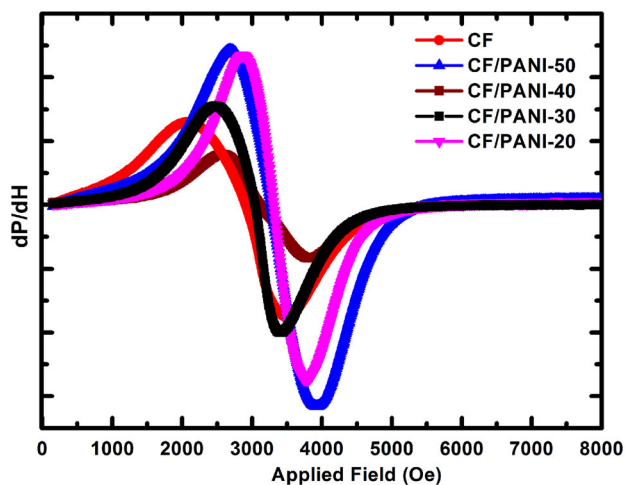


Fig. 11. ESR spectra for the CF/PANI nanocomposites obtained at room temperature.

interactions existing among the fine clusters of cobalt ferrite, and this can cause ΔH_{PP} to decrease.³⁰

The spin–spin relaxation process is the energy difference (ΔE) transferred to neighbouring electrons and the relaxation time (T_2) can be determined from the peak-to-peak line width according where β is the Bohr magneton (9.274×10^{-21} ergG⁻¹), $\Delta H_{1/2}$ is the line width (in Oe) at half-height of the absorption peak and h is a constant (1.054×10^{-27} erg s⁻¹).³⁰ The relaxation time of the EPR signal is directly related to the interactions of the spins with their environment and to their motion. In our case, the values of ΔH_{PP} and g factor of the CF/PANI nanocomposites decreased with an increase of PANI, whereas the T_2 value was converse (Table VIII). Moreover, T_2 increased with an increase of PANI, indicating that the delocalization of polarons in PANI was increased in the cobalt ferrite. These results may be due to the interaction between the PANI and CoFe_2O_4 influencing the motion of π -electrons in PANI.³⁰

CONCLUSIONS

A series of CoFe_2O_4 loading in PANI polymer matrix nanocomposites were prepared at room temperature. The x-ray diffraction studies confirm the phase formation. The particle size from TEM for CoFe_2O_4 and CF/PANI-30 was 20 nm and 24 nm, respectively. The grain size of all the nanocomposites was found to be in the range of 45–68 nm. As the ferrite content increases in the composite, the saturation magnetization increased, whereas coercivity values remain constant. Saturation magnetization of CF/PANI composites were less than that of CoFe_2O_4 , indicating an increase of ferromagnetic interaction with more incorporation of cobalt ferrite in PANI matrix, whereas PANI is diamagnetic. The composites exhibit broadband absorptive characteristics, possibly caused by the extended resonance due to an overlap between imaginary permeability and permittivity of the nanocomposites over the frequency range from 2 GHz to 20 GHz. Polyaniline-based nanocomposites clearly reveal that they can be efficiently used as EMI shielding materials. These materials find applications in mobile phones for reducing the specific absorption rate (SAR). Because of their high EMI shielding efficiency,

Table VIII. Data of EPR parameters for CF/PANI with different PANI loadings

Sample name	ΔH_{PP} (Oe)	g	Relaxation time (T_2) (10^{-11}) s
CF	1397	2.10	2.33
CF/PANI-50	1219	2.22	2.67
CF/PANI-40	1199	2.25	2.72
CF/PANI-30	923	2.46	3.53
CF/PANI-20	917	2.67	3.56
CF/PANI-10	–	–	–

these materials can be used in electromagnetic compatibility studies and as material for anechoic chambers.

CONFLICTS OF INTEREST

The authors declare that they have no conflict of interest.

ELECTRONIC SUPPLEMENTARY MATERIAL

The online version of this article (<https://doi.org/10.1007/s11664-020-08352-y>) contains supplementary material, which is available to authorized users.

REFERENCES

1. K. Praveena, S. Matteppanavar, H.-L. Liu, and K. Sadhana, *J. Mater. Sci. Mater. Electron.* 28, 4179 (2017).
2. K. Praveena, K. Sadhana, H.L. Liu, N. Maramu, and G. Himanandini, *J. Alloys Compd.* 681, 499 (2016).
3. C. Pan, K. Kou, Y. Zhang, Z. Li, and G. Wu, *Compos. Part B-Eng.* 153, 1 (2018).
4. P. Song, Z. Xu, Y. Wu, Q. Cheng, Q. Guo, and H. Wang, *Carbon* 111, 807 (2017).
5. J. Liu, H. Zhang, R. Sun, Y. Liu, Z. Liu, A. Zhou, and Z.-Z. Yu, *Adv. Mater.* 29, 1702367 (2017).
6. P. Gairola, L.P. Purohita, S.P. Gairolab, P. Bhardwajb, and S. Kaushik, *Prog. Nat. Sci. Mater. Int.* 29, 170 (2019).
7. C. Wang, V. Murugadoss, J. Kong, Z. He, X. Mai, Q. Shao, Y. Chen, L. Guo, C. Liu, S. Angaiah, and Z. Guo, *Carbon* 140, 696 (2018).
8. Z. Wang, R. Wei, J. Gu, H. Liu, C. Liu, C. Luo, J. Kong, Q. Shao, N. Wang, Z. Guo, and X. Liu, *Carbon* 139, 1126 (2018).
9. H. Lv, H. Zhang, G. Ji, and Z.J. Xu, *ACS Appl. Mater. Interfaces* 8, 6529 (2016).
10. K. Praveena, K. Sadhana, S. Matteppanavar, and H.L. Liu, *J. Magn. Magn. Mater.* 423, 343 (2017).
11. K. Praveena, K. Sadhana, H.L. Liu, and S.R. Murthy, *J. Mater. Sci. Mater. Electron.* 27, 12680 (2016).
12. M. Fayzan Shakir, A. Tariq, Z.A. Rehan, Y. Nawab, I. Abdul Rashid, A. Afzal, U. Hamid, F. Raza, K. Zubair, M. Saad Rizwan, S. Riaz, A. Sultan, and M. Muttaqi, *SN Appl. Sci.* 2, 1 (2020).
13. C. Oueiny, S. Berlioz, and F.-X. Perrin, *Prog. Polym. Sci.* 39, 707 (2014).
14. X. Xiaojiang, F. Qiangang, G. Hongbo, Y. Guo, H. Zhou, J. Zhang, D. Pan, W. Shide, M. Dong, and Z. Guo, *Polymer* 188, 122129 (2020).
15. A. Mohamed Azharudeen, R. Karthiga, M. Rajarajan, and A. Suganthi, *Arab. J. Chem.* 13, 4053 (2020).
16. H. Hosseini, A. Zirakjou, V. Goodarzi, S. Mohammad Mousavi, H. AliKhonekdar, and S. Zamanlui, *Int. J. Biol. Macromol.* 152, 57 (2020).
17. H. Wei, H. Gu, J. Guo, D. Cui, X. Yan, J. Liu, D. Cao, X. Wang, S. Wei, and Z. Guo, *Adv. Compos. Hybrid Mater.* 1, 127 (2018).
18. B. Saravanakumar, G. Ravi, R.K. Guduru, and R. Yuvakkumar, *J. Sol-Gel Sci. Technol.* 94, 241 (2020).
19. A.I. Gopalan, S. Komathi, N. Muthuchamy, K.P. Lee, M.J. Whitcombe, L. Dhana, and G. Sai-Anand, *Prog. Polym. Sci.* 88, 1 (2019).
20. W. Zhang, X. Zhang, Z. Wu, K. Abdurahman, Y. Cao, H. Duan, and D. Jia, *Compos. Sci. Technol.* 188, 107966 (2019).
21. H. Gu, H. Zhang, J. Lin, Q. Shao, D.P. Young, L. Sun, T.D. Shen, and Z. Guo, *Polymer* 143, 324 (2018).
22. M. Saini, R. Shukla, and S.K. Singh, *J. Inorg. Organomet. Polym. Mater.* 29, 2044 (2019).
23. M. Saini, R. Shukla, and A. Kumar, *J. Magn. Magn. Mater.* 491, 165549 (2019).
24. H. Qiu, X. Luo, J. Wang, X. Zhong, and S. Qi, *J. Electron. Mater.* 48, 4400 (2019).
25. C. Yang, J. Jiang, X. Liu, C. Yin, and C. Deng, *J. Magn. Magn. Mater.* 404, 45 (2016).
26. M. Wang, G. Ji, B. Zhang, D. Tang, Y. Yang, and D. Youwei, *J. Magn. Magn. Mater.* 377, 52 (2015).
27. S.P. Gairola, V. Verma, L. Kumar, M. Abdullah Dar, S. Annapoorni, and R.K. Kotnala, *Synth. Met.* 160, 2315 (2010).
28. H. Yang, T. Ye, and Y. Lin, *RSC Adv.* 5, 103488 (2015).
29. S.H. Hosseini, S.H. Mohseni, A. Asadnia, and H. Kerdari, *J. Alloys Compd.* 509, 4682 (2011).
30. T.H. Ting, R.P. Yu, and Y.N. Jau, *Mater. Chem. Phys.* 126, 364 (2011).
31. C. Wang, Y. Shen, X. Wang, H. Zhang, and A. Xie, *Mater. Sci. Semicond. Proc.* 16, 77 (2013).
32. A. Muñoz-Bonilla, J. Sánchez-Marcos, and P. Herrasti, *Conducting Polymer Hybrids* Springer Series on Polymer and Composite Materials, (Cham: Springer, 2017), p. 45.
33. R.T. Ma, H.T. Zhao, and G. Zhang, *Mater. Res. Bull.* 45, 1064 (2010).
34. J.M.A. Sulaiman, M.M. Ismail, S.N. Rafeeq, and A. Mandal, *Appl. Phys. A* 126, 236 (2020).
35. H.K. Choudhary, R. Kumar, S.P. Pawar, S. Bose, and B. Sahoo, *J. Electron. Mater.* 49, 1618 (2020).
36. Y. Zhang, L. Wang, J. Zhang, P. Song, Z. Xiao, C. Liang, H. Qiu, J. Kong, and G. Junwei, *Compos. Sci. Technol.* 183, 107833 (2019).
37. X. Yang, S. Fan, Y. Li, Y. Guo, Y. Li, K. Ruan, S. Zhang, J. Zhang, J. Kong, and G. Junwei, *Compos. Part A Appl. Sci. Manuf.* 128, 105670 (2020).
38. P. Song, H. Qiu, L. Wang, X. Liu, Y. Zhang, J. Zhang, J. Kong, and J. Gu, *Sustain. Mater. Technol.* (2020). <https://doi.org/10.1016/j.susmat.2020.e00153>.
39. T. Pan, Y. Zhang, C. Wang, H.G.B. Wen, and B. Yao, *Compos. Sci. Technol.* 188, 107991 (2020).
40. X. Yang, X. Wang, and Z. Zhang, *J. Cryst. Growth* 277, 467 (2005).
41. K. Sadhana, K. Praveena, and S.R. Murthy, *Mod. Phys. Lett. B* 24, 369 (2010).
42. K. Sadhana, R. Sandhya, S.R. Murthy, and K. Praveena, *Mater. Focus* 3, 291 (2014).
43. K. Praveena, K. Sadhana, and S.R. Murthy, *Integr. Ferroelectr.* 119, 122 (2010).
44. S.R. Naik, A.V. Salker, and J. Mater, *Chem.* 22, 2740 (2012).
45. M. Artus, L.B. Tahar, F. Herbst, L. Smiri, F. Villain, N. Yaacoub, J.-M. Grenèche, S. Ammar, and F. Fiévet, *J. Phys. Condens. Matter.* 23, 506001 (2011).
46. M. Khandekar, R. Kambale, J. Patil, Y. Kolekar, and S. Suryavanshi, *J. Alloys Compd.* 509, 1861 (2011).
47. A.H. Lu, E.L. Salabas, and F. Schuth, *Angew. Chem. Int. Ed.* 46, 1222 (2007).
48. E. Manova, B. Kunev, D. Paneva, I. Mitov, and L. Petrov, *Chem. Mater.* 16, 5689 (2004).
49. K. Praveena and S. Srinath, *J. Nanosci. Nanotechnol.* 14, 4371 (2014).
50. W.B. Weir, *Proc. IEEE* 62, 33 (1974).
51. A.M. Nicolson and G.F. Ross, *IEEE Trans. Instrum. Meas.* 19, 377 (1970).
52. S.B. Wilson, *IEEE Trans. Microw. Theory Technol.* 36, 752 (1988).
53. D. Micheli, R. Pastore, C. Apollo, M. Marchetti, G. Gradoni, V.M. Primiani, and F. Moglie, *IEEE Trans. Microw. Theory Technol.* 59, 2633 (2011).
54. D. Micheli, A. Vricella, R. Pastore, and M. Marchetti, *Carbon* 77, 756 (2014).
55. K.H. Wu, Y.M. Shin, C.C. Yang, W.D. Ho, and J.S. Hsu, *J. Polym. Sci. Part A Polym. Chem.* 44, 2657 (2006).
56. N. Gandhi, K. Singh, A. Ohlan, D.P. Singh, and S.K. Dhanwan, *Compos. Sci. Technol.* 71, 1754 (2011).

57. L. Li, H. Qiu, H. Qian, B. Hao, and X. Liang, *J. Phys. Chem. C* 114, 6712 (2010).
58. W. Wang, S.P. Gumfekar, Q. Jiao, and B. Zhao, *J. Mater. Chem. C* 1, 2851 (2013).
59. S.M. Abbas, A.K. Dixit, R. Chatterjee, and T.C. Goel, *J. Magn. Magn. Mater.* 309, 20 (2007).
60. A. Ameli, S. Wang, Y. Kazemi, C.B. Park, and P. Pötschke, *Nano Energy* 15, 54 (2015).
61. J.Y. Kim, T. Kim, J.W. Suk, H. Chou, J.H. Jang, J.H. Lee, I.N. Kholmanov, D. Akinwande, and R.S. Ruoff, *Small* 10, 3405 (2014).
62. L.F. Malmonge, G.A. Lopes, S.D.C. Langiano, J.A. Malmonge, J.M.M. Cordeiro, and L.H.C. Mattoso, *Eur. Polym. J.* 42, 3108 (2006).
63. S.M. Abbas, M. Chandra, A. Verma, R. Chatterjee, and T.C. Goel, *Compos. A* 37, 2148 (2006).
64. V. Truong, S.Z. Riddell, and R.F. Muscat, *J. Mater. Sci.* 3, 4974 (1998).
65. Z. Sun, F. Su, W. Forsling, and P. Samskog, *J. Colloid Interface Sci.* 197, 155 (1998).
66. T. Giannakopoulou, L. Kompotiatis, A. Kontogeorgakos, and G. Kordas, *J. Magn. Magn. Mater.* 246, 360 (2002).
67. P. Liu, V.M.H. Ng, Z. Yao, J. Zhou, Y. Lei, Z. Yang, and L.B. Kong, *J. Alloys Compd.* 701, 841 (2017).
68. P. Liu, Z. Yao, J. Zhou, Z. Yang, and L.B. Kong, *J. Mater. Chem. C* 4, 9738 (2016).
69. L.-C. Jia, D.-X. Yan, X. Liu, R. Ma, W. Hong-Yuan, and Z.-M. Li, *ACS Appl. Mater. Interfaces* 10, 11941 (2018).
70. L. Wang, L. Chen, P. Song, C. Liang, L. Yuanjin, H. Qiu, Y. Zhang, J. Kong, and G. Junwei, *Compos. Part B Eng.* 171, 111 (2019).
71. L.-X. Liu, W. Chen, H.-B. Zhang, Q.-W. Wang, F. Guan, and Yu Zhong-Zhen, *ACS Adv. Funct. Mater.* 29, 1905197 (2019).
72. P. Song, C. Liang, L. Wang, H. Qiu, G. Hongbo, J. Kong, and G. Junwei, *Compos. Sci. Technol.* 181, 107698 (2019).
73. Z. Shen and J. Feng, *ACS Sustain. Chem. Eng.* 7, 6259 (2019).
74. C. Liang, P. Song, A. Ma, X. Shi, G. Hongbo, L. Wang, H. Qiu, J. Kong, and G. Junwei, *Compos. Sci. Technol.* 181, 107683 (2019).
75. L. Wang, H. Qiu, P. Song, Y. Zhang, L. Yuanjin, C. Liang, J. Kong, L. Chen, and G. Junwei, *Compos. Part A Appl. Sci. Manuf.* 123, 293 (2019).
76. I.Y. Sakharov, I.V. Ouporov, A.K. Vorobiev, M.G. Roig, and O.Y. Pletjushkina, *Synth. Met.* 142, 127 (2004).
77. H.K. Liu, C.C. Shih, G.P. Wang, T.R. Wu, K.H. Wu, and T.C. Chang, *Synth. Met.* 151, 256 (2005).

Publisher's Note Springer Nature remains neutral with regard to jurisdictional claims in published maps and institutional affiliations.